Net section resistance in bolted cold-formed steel angles under tension, Journal of Constructional Steel Research, https://doi.org/10.1016/j.jcsr.2019.105841

Manuscript …

Net section resistance in bolted cold-formed steel angles under tension

Israel Fleitas[(a)], Jorge Bonilla[(a),(b)], Luciano M. Bezerra[(b),(*)], Enrique Mirambell[(c)]

[(a)] Group for Numerical Methods in Engineering, University of Ciego de Ávila, Cuba
[(b)] Department of Civil & Environmental Engineering, University of Brasília, Brazil
[(c)] Department of Civil and Environmental Engineering, Polytechnic University of Catalunya, Spain
[(*)] Corresponding author. E-mail address: lmbz@unb.br

Abstract. Net section resistance in bolted cold-formed steel angles of members under tension is analyzed in this work. The efficiency reduction due to shear lag and eccentricity effects in bolted connections is studied using finite element models implemented in ABAQUS software. The nonlinearities of the steel material and the contact between elements are considered in the numerical models, and their results are in good agreement with experimental tests. A parametric study is conducted in this work using Finite Element (FE) analyses. A large number of experimental tests reported in the literature is also summarized in this work. A new expression of easy application for net section reduction coefficient is found, which allows improving the prediction of the nominal resistance of the net section.

Keywords: Bolted connections; Shear lag; Net section failure; Cold-formed steel angles; Tensile strength.

1. Introduction

The stress state that involves the bolted connection under tension is very complex, and the net section resistance cannot be computed, in many cases, as the product of material tensile strength and net section area. When cold-formed angles are used, it is usual to connect only one of the two legs to the gusset plate. In such cases, stress distribution in the cross-sectional area of the cold-formed angle is not uniform. In these cases, a phenomenon known as shear lag occurs, reducing the efficiency of the connection.

The shear lag phenomenon is observed in bolted connections of hot rolled steel angles, as well as in cold-formed angle connections. Munse and Chesson [1] developed 218 tests with different cross-sectional configurations, connections, materials and fabrication methods. An empirical equation to calculate the net section efficiency was proposed. The equations of various design standards [2–4] were fundamentally based on the aforementioned research [1]. Laboube and Yu [5] proposed a very practical expression to determine the reduction coefficient for the net section in bolted connections of cold-formed steel angles under tension. This expression is simple to use and was adopted by the North American Standard [2,3].

Kulak and Wu [6] developed 24 tests of bolted connections of members with single and double angle under tension. FE analysis was used by the authors [6] to obtain a prediction of the connection resistance and evaluate the stress distribution at the critical cross-section. An equation for the prediction of the net section strength for single or double angle members was proposed. More recently, de Paula et al. [7] developed 66 experimental tests of bolted connections of cold-formed steel angle members under tension. As result of that research, a new equation for net section reduction coefficient was proposed. Teh and Yazici [8] performed 55 tests of bolted connections of cold-formed channel members with single and back-to-back channel braces. Based on the research above, the authors proposed several design recommendations for bolted connections using cold-formed channels. Teh and Gilbert [9] developed 61 tests of bolted connections that include: single equal angle, single unequal angle bolted at the wider leg, single unequal angle bolted at the narrow leg, double angles, and alternate angles. A new equation for net section reduction coefficient was proposed by the authors [9].

In this research, the predictions of the nominal resistance of the net section obtained from AISI [10] and Eurocode-3 [11] are compared with a large number of experimental results available in the literature [7,9,12,13].

An accurate and efficient nonlinear FE model to investigate the efficiency reduction due to shear lag of bolted connections in cold-formed angles under tension is developed in this research. For this purpose, FE modeling using ABAQUS [14] software is employed. The nonlinearities of the steel material and the contact between elements are considered in the numerical models. The results obtained from FE analyses have been verified against experimental test results available in the literature [7,9,12,13]. In the present research, a parametric study is conducted using FE analyses to investigate the effect of the connected length in the longitudinal direction and in the transverse direction, as well as, the effect of the eccentricities in $\bar{x}$ and $\bar{y}$ directions on connection efficiency. As result of this research, a new equation for the efficiency coefficient prediction of the net section area of cold-formed steel angles under tension is proposed.

Notation

The following symbols are used in this paper:

A_{nt}, A_n Net section area.
F_u Ultimate tensile strength of the steel material.
L Length of connection in the longitudinal direction (see Fig. 7).
L_t Length of connection in the transverse direction (see Fig. 7).
P_u Ultimate capacity of the net section [10].
T_{AISI}, P_{nt} Nominal resistance of the net section calculated according to AISI [10].
T_{EC-3} Nominal resistance of the net section calculated according to Eurocode-3 [11].
$T_{Eq. (7)}$ Nominal resistance of the net section calculated using the new Eq. (6).
T_{FE} Resistance of the net section calculated using the FE analysis.
T_{exp} Resistance of the net section obtained from the experimental test.
$N_{u,Rd}$ Design ultimate resistance of the net section [11].
U_{sl} Net section reduction coefficient calculated according to AISI [10].
U_e Net section reduction coefficient proposed in this work.
U_{exp} Experimental coefficient of net section reduction, calculated as $T_{exp}/A_n F_u$.
U_{FE} Net section reduction coefficient obtained from FE analysis, calculated as $T_{FE}/A_n F_u$.
b_2, b_c Width of the angle connected leg.
b_1, b_d Width of the not connected leg.
d Nominal bolt diameter.
d_0 Hole diameter for a bolt.
e_2 The edge distance from the centers of a fastener hole to the adjacent edge of any part, measured at right angles to the direction of load transfer.
f_y Yield strength of the steel material.
f_u Specified ultimate tensile strength of the steel material.
p_1 Spacing between centers of fasteners in a line in the direction of load transfer.
t Angle thickness.
$\bar{x}$ Connection eccentricity. Distance from shear plane to the centroid of the cross-section (see Fig. 7).
$\bar{y}$ Connection eccentricity. Distance from the centroid of the connection to the centroid of cross-section measured in a line in "y" axis direction (see Fig. 7).

2. Procedures according to current design standards

In this section, the procedures according to AISI [10] and Eurocode-3 [11] to estimate the ultimate capacity of the net section in cold-formed steel angles under tension are presented.

The AISI [10] equation for the prediction of ultimate capacity of the net section is given by:

$$P_u = \emptyset\, P_{nt} \quad \text{with} \quad P_{nt} = U_{sl} \cdot A_{nt} \cdot F_u \tag{1}$$

where the ultimate capacity P_u is obtained from the nominal resistance P_{nt} factored by a coefficient $\emptyset$. In Eq. (1), the reduction coefficient U_{sl} which takes into account the shear lag in bolted connections of cold-formed steel angles under tension was established based on research studies developed by Teh and Gilbert [15]. Based in such research, AISI [10] stated that the coefficient U_{sl} can be determined according to Eq. (2).

$$U_{sl} = \frac{1}{1.1 + \frac{0.5b_1}{b_2 + b_1} + \frac{2\bar{x}}{L}} \tag{2}$$

According to Eurocode-3 [11], a single angle in tension connected by a single row of bolts in one leg may be treated as concentrically loaded over an effective net section for which the design ultimate resistance should be determined as follows:

With one bolt: $$N_{u,Rd} = \frac{2.0(e_2 - 0.5d_0)t\, f_u}{\gamma_{M2}} \tag{3}$$

With two bolts: $$N_{u,Rd} = \frac{\beta_2\, A_n\, f_u}{\gamma_{M2}} \tag{4}$$

With three or more bolts: $$N_{u,Rd} = \frac{\beta_3\, A_n\, f_u}{\gamma_{M2}} \tag{5}$$

The variables in Eqs.(3), (4), and (5) are in the notation table, and the reduction factors β_2 and β_3 are summarized in table 1.

Table 1. Values of reduction factors β_2 and β_3.

Pitch p_1	$\leq 2.5d_0$	$\geq 5d_0$
β_2 for two bolts	0.4	0.7
β_3 for three or more bolts	0.5	0.7

Note: For intermediate values of pitch p_1 the value of β is determined by linear interpolation.

3. Numerical simulation of the test of bolted cold-formed angles under tension

In this section, the numerical simulation of the test of bolted cold-formed angles under tension is presented. For that purpose, FE analysis using ABAQUS software is performed. The geometric nonlinearity, the contact between different parts (bolt, cold-formed angle, and gusset plate) and material nonlinearity are introduced in the FE numerical model.

3.1 Specimen configuration for the bolted cold-formed angles test under tension

This study is based on the virtual simulation of the bolted cold-formed angles test under tension. Firstly, the calibration of the FE model is developed using the specimen test C122 of de Paula et al. [7] and then the verification of the FE model is conducted with others specimens from the same author [7] and others authors too [7,9,12,13]. The specimen C122 consists of an angle section with equal legs of 100 x 100 mm and a thickness of 2.66 mm, connected to a 12.7 mm thick gusset plate at the end by four bolts of diameter 12.7 mm (1/2”) (see Fig. 1). The angle section was made from a steel known in the Brazilian industry as COR-420 [7]. All bolts are ASTM A325 and tightened with a torquing moment of 100 N-m. Bolts are used in 1.5 mm clearance holes.

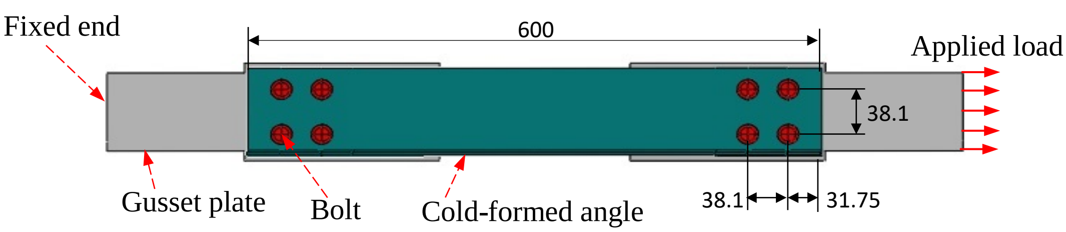

Fig. 1 Description of test specimen C122 [7]

3.2 Material modeling of steel

For modeling of steel material, a von Mises’ criterion was adopted. The option (*PLASTIC) available in ABAQUS [14] was utilized. ABAQUS uses the classic rule of associated plastic flow and the isotropic yielding [14,16] to represent the behavior of steel material in the three-dimensional (3D) space of stresses. To simulate the 3D behavior of the steel material accurately, ABAQUS [14,16] just needs the steel uniaxial stress-strain curve which is represented, in this research, by the trilinear stress-strain curve shown in Fig. 2. In this curve, the steel material behavior is initially elastic with Young's modulus (*Es*) followed by strain hardening and then yielding. In this analysis, E_s, f_y, F_u and ε_u were taken as 210000 MPa, 368 MPa, 502 MPa, and 28.6 %, respectively [7,17].

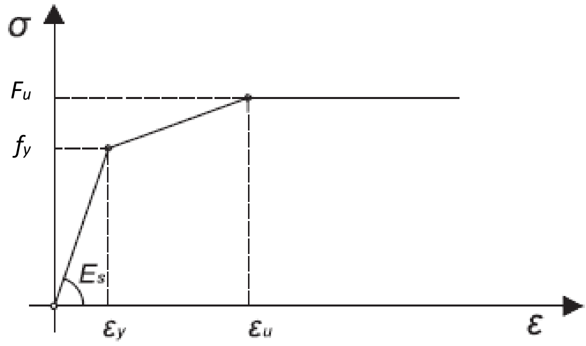

Fig. 2. Stress–strain relationship for steel material.

3.3 Finite element type and mesh

Solid elements which are available in the ABAQUS [14] element library, are used to model all parts of the connection test specimens. Six-node elements (SC6R) and (C3D6), and eight-node elements (C3D8R) are used to model the cold-formed angle, the gusset plates, and the bolts, respectively (see Fig. 3). The elements were chosen according to the need to capture the nonlinear behavior (geometry or material) [14]. For instance, to model contact and other nonlinearities, the continuum shell element (SC6R) was used as it is very accurate compared to C3D8R and C3D6 elements – for more details see suggestions in [14]. The definition of the FE meshes and elements for each region is done according to the expected stress gradient and to linear or nonlinear regimes [14]. The meshes in the cold-formed angle and the gusset plate are employed with variable FE density, refining the mesh towards the angle-bolt and gusset plate-bolt contact area due to stress gradients. The mesh has a uniform size in the bolts. To avoid numerical inaccuracies, the shape of the elements satisfies the limits and the aspect ratio for solid elements as recommended by ABAQUS [14]. In order to make easy the modelling process, bolts with circular heads were considered in the numerical simulations (see Fig. 3).

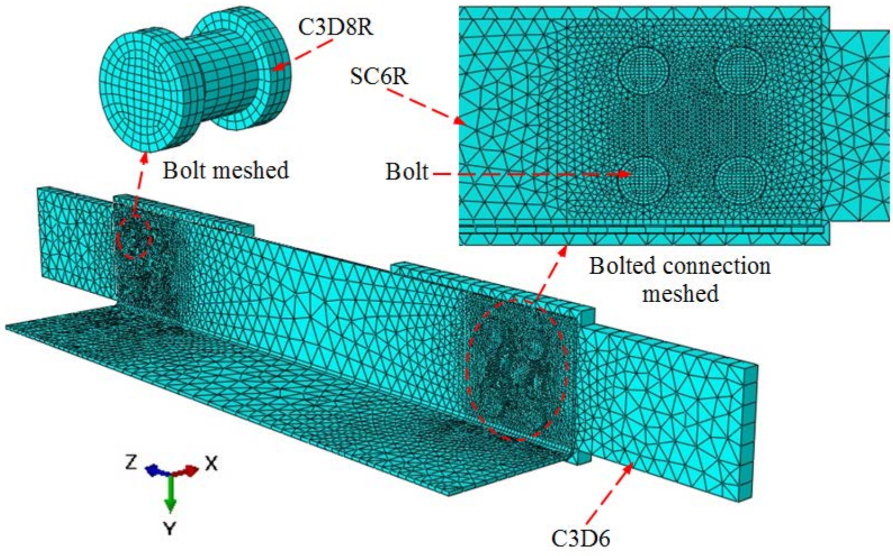

Fig. 3. Finite element mesh of the model.

3.4 Application of boundary conditions

The load is applied on surface 1 in small increments (see Fig. 4). The size of the load increments is automatically selected by ABAQUS [14,16], based on the condition of numerical convergence using the modified RIKS algorithm in ABAQUS [14,16]. All nodes of surface 2, at the end of the gusset plate, are restricted from moving in the axes directions X, Y, and Z. The bolt load considered in the numerical model also considered the tightening torque of 100 N-m applied in each bolt as done in the experimental test [7,17]. The option *"Bolt load"* available in the load module in ABAQUS [14] was utilized to model the effect of the tightening torque.

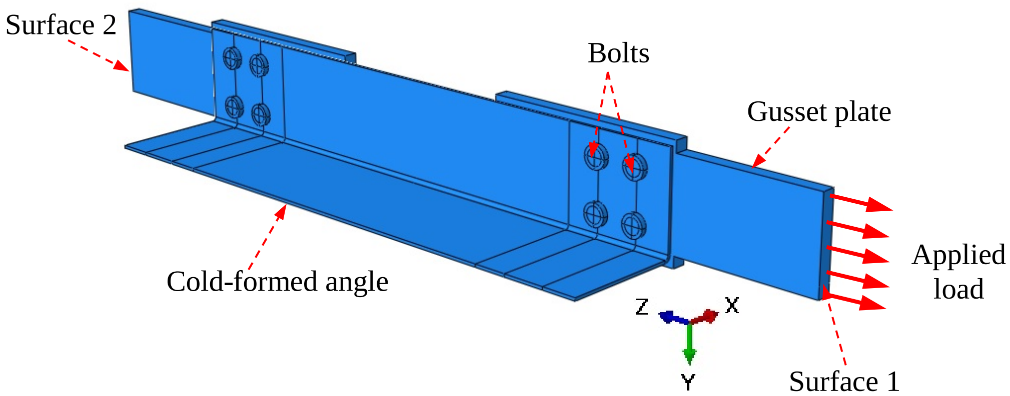

Fig. 4. Load and boundary conditions.

3.5 Contact surfaces

There are three surfaces of interaction: the angle-gusset plate interface, the angle-bolt interface, and the gusset plate-bolt interface. In all cases, a surface-to-surface contact was defined, following a small sliding approach for the angle-gusset plate and the angle-bolt interfaces. The angle-gusset plate and angle-bolt interactions were defined through the normal and tangential contact surface interactions. The default contact option in ABAQUS [14] was considered, which consists of a hard contact pressure-over closure relationship. Regarding the tangential direction, the penalty frictional formulation with a friction coefficient equal to 0.2 was employed [11,18,19]. Alternatively, the interaction between the gusset plate and the bolts was defined as a rigid contact by means of the (*TIE) constraint available in ABAQUS [14].

4. Verification of the finite element model

In the previous sections, the procedure and considerations to develop the FE model were explained based on the test specimen C122 of de Paula et al.[7]. In this section, other test specimens conducted by several authors [7,9,12,13] are used to verify the accuracy of the FE model. Table 2 summarizes the measured dimensions of theses tested specimens and shows a comparison of the connection resistance obtained experimentally and numerically. It can be seen a good agreement between numerical and experimental results. A maximum T_{exp}/T_{FE} ratio of 1.073 between experimental and numerical results was obtained for the test of the specimen C212. The mean value of the T_{exp}/T_{FE} ratio is 1.001 with a corresponding coefficient of variation (COV) of 0.033 (see Table 2).

The experimental load-displacement curves obtained for the specimens C122 and C212 were compared with the numerical curves obtained from the FE analysis, as shown in Fig. 5. Good agreement has been achieved between experimental and numerical load-displacement curves. It can be observed that the FE models successfully predicted the resistance of bolted connection under tension and its load-displacement behavior.

Table 2. Specimens for the verification of finite element model.

Tested by	Specimen	Number of bolt lines	No. of holes per bolt line	b_c - b_d - t (mm)	T_{exp} (kN)	T_{FE} (kN)	T_{exp}/ T_{FE}
de Paula et al.[7]	A241[(a)(L1)]	1	4	50 – 50 - 3.57	102.00	103.28	0.987
	B142[(b)(L1)]	2	4	80 – 80 - 2.43	109.18	107.93	1.012
	C122[(b)(L1)]	2	2	100 – 100 – 2.66	99.56	105.85	0.941
	C212[(a)]	2	1	100 – 100 – 3.58	94.27	87.89	1.073
	E121[(b)(L1)]	1	2	50 – 100 – 2.49	64.36	62.17	1.035
Holcomb and Yu [12]	LBN11[(c)(L1)]	1	2	41.3 – 41.3 – 1.07	15.97	16.21	0.985
	LCN12[(c)(L1)]	1	3	41.3 – 82.5 – 1.07	22.35	22.12	1.010
Yip and Cheng [13]	l2.2[(d)(L3)]	1	2	102 – 102 - 2.65	135.8	137.01	0.991
	l4.2[(e)(L5)]	1	2	50.8 – 50.8 – 1.89	35.70	34.91	1.023
Teh and Gilbert [9]	EA1[(f)(L2)]	1	2	40 – 40 – 3.00	(*)	36.01	0.973
	EA24[(f)(L6)]	1	2	75 – 75 – 3.00	(*)	123.75	0.981
	UAN5[(f)(L4)]	1	2	40 – 80 – 3.00	(*)	93.11	1.003
						Mean	1.001
						COV	0.033

Note: The ultimate tensile strength (F_u) of the cold-formed angle is 463 MPa[(a)], 502 MPa[(b)], 385 MPa[(c)], 516 MPa[(d)], 327 MPa[(e)] and 580 MPa[(f)]. The nominal bolt diameter is 12.7 mm (1/2”) for all specimens. The distance between sequential bolts is (in mm): 38.1[(L1)], 40[(L2)], 95.5[(L3)], 60[(L4)] 63.3[(L5)] and 100[(L6)].
[(*)] The value of T_{exp} is not reported by the authors in [9], hovewer, the ratio T_{exp}/T_n is reported in [9]. In that scence, T_{exp} is estimated, aproximetly, by $T_{exp} = (T_{exp}/T_n) \cdot U_e \cdot A_n \cdot F_u$.

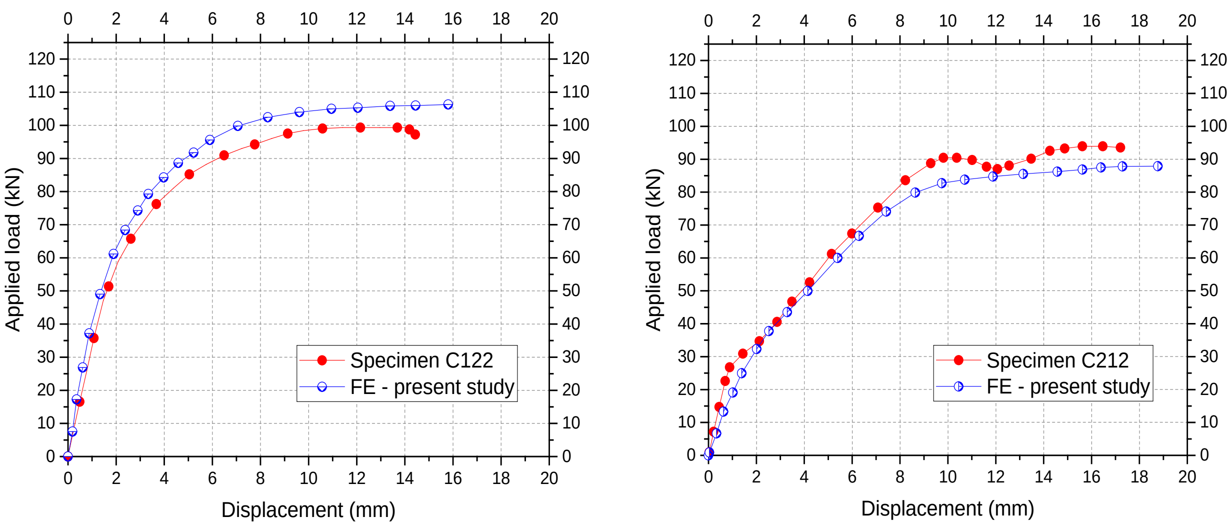

Fig. 5. Load versus displacement curves for specimens C122 and C212 [7].

The stress distribution near the bolted connection is complex. Fig. 6 shows the deformed shape and the stress contour (in Pa) of specimen C122 at failure obtained numerically. Fig. 6 also shows the deformed shape of the specimen after the experimental test. Good agreement between numerical and experimental results is observed. It should be noted that the maximum von Mises stresses in the cold-formed angle are in the regions around the holes. High stress concentration between the holes 1 and 4 can be observed in the numerical model and in the experimental test [7].

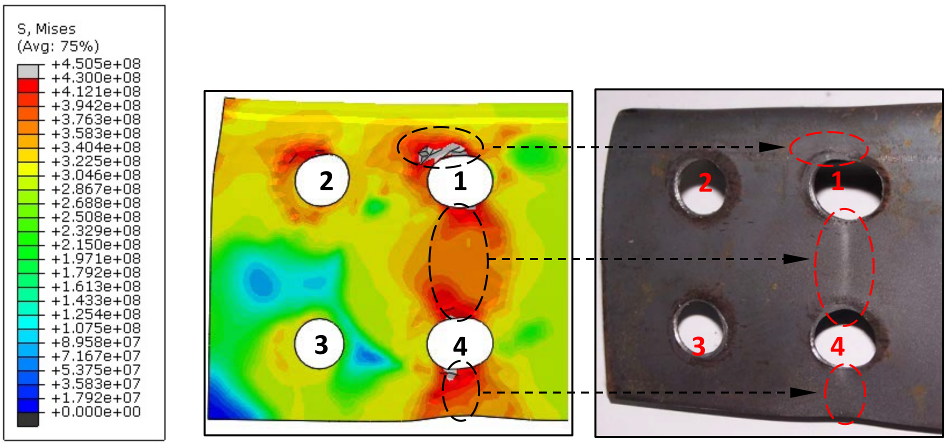

Fig. 6. Stress contour and detail of net section failure of specimen C122 [7].

5. Study of different factors influencing the bolted connection behavior

5.1 Effect of connected length on connection efficiency

Effect of the connected length in the longitudinal direction (L) and the transverse direction (L_t) on the efficiency of the connection is analyzed in this section. Fig. 7 shows the distances L and L_t for a typical bolted connection of cold-formed angle.

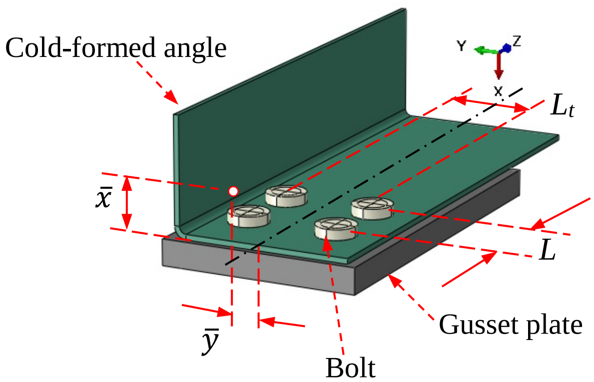

Fig. 7. Typical bolted connection in cold-formed angle

For the analysis of the influence of the connected length L on connection efficiency, a specimen of cold-formed angle with legs of 100 x 100 mm and thickness of 2.66 mm connected to the gusset plate by using four bolts of diameter 12.7 mm was numerically modeled (see Fig. 7). Connected length L was incremented in a range between 33 and 76 mm and an increase in connection efficiency was observed. A quasi-linear relation between U_{FE} ($U_{FE} = T_{FE}/A_n F_u$) and L is exhibited, as can be seen in Fig. 8(a). A linear fit was developed with a coefficient of determination (R^2) of 0.982 for verifying such behavior.

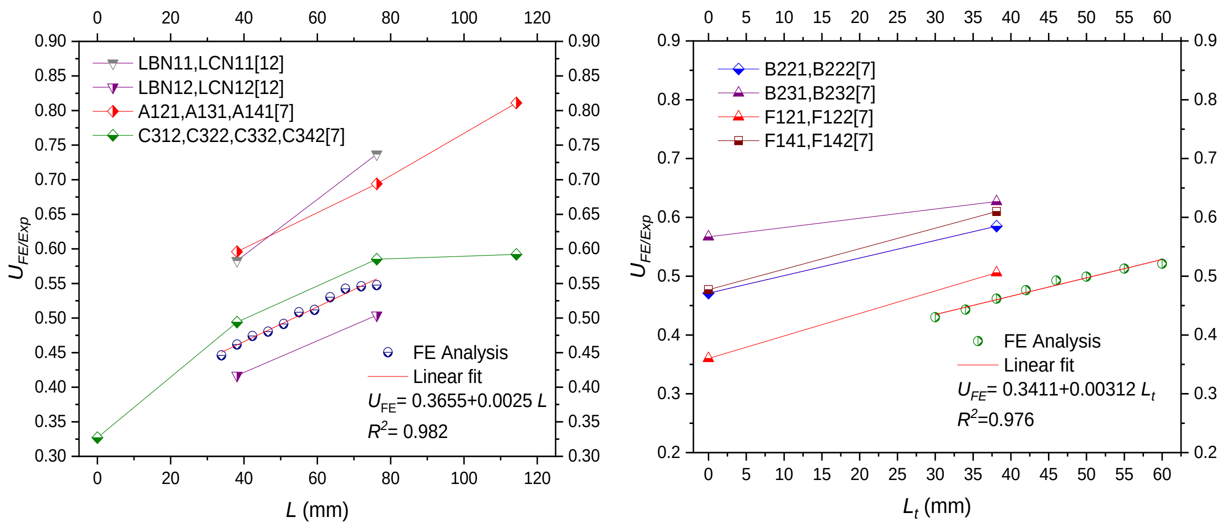

Fig. 8. Effect of connected lengths in: (a) Longitudinal direction, and (b) Transverse direction.

Table 3. Effect of length L and L_t on connection efficiency for different experimental tests.

Tested by	Specimen	Number of bolt lines	No. of holes per bolt line	b_c - b_d - t (mm)	L (mm)	L_t (mm)	U_{exp} (1)
Holcomb and Yu [12]	LBN11	1	2	41.3 – 41.3 – 1.07	38.1	-	0.583(*)
	LCN11	1	3		76.2	-	0.737(*)
	LBN12	1	2	41.3 – 82.5 – 1.07	38.1	-	0.417(*)
	LCN12	1	3		76.2	-	0.504(*)
de Paula et al.[7]	A121	1	2	50 – 50 – 2.23	38.1	-	0.596
	A131	1	3	50 – 50 – 2.26	76.2	-	0.694
	A141	1	4	50 – 50 – 2.34	114.3	-	0.811
	C312	2	1	100 – 100 – 3.86	0.0	38.1	0.327
	C322	2	2	100 – 100 – 3.86	38.1		0.494
	C332	2	3	100 – 100 – 3.85	76.2		0.585
	C342	2	4	100 – 100 – 3.84	114.3		0.592
de Paula et al.[7]	B221	1	2	80 – 80 – 3.54	38.1	-	0.471
	B222	2	2	80 – 80 – 3.50		38.1	0.585
	B231	1	3	80 – 80 – 3.55	76.2	-	0.567
	B232	2	3	80 – 80 – 3.53		38.1	0.627
	F121	1	2	80 – 100 – 2.34	38.1	-	0.360
	F122	2	2	80 – 100 – 2.46		38.1	0.506
	F141	1	4	80 – 100 – 2.30	114.3	-	0.477
	F142	2	4	80 – 100 – 2.38		38.1	0.610

Note: The nominal bolt diameter is 12.7 mm (1/2”) for all specimens.
(*) Average in the series.
(1) $U_{exp}=T_{exp}/A_n F_u$

Table 3 summarizes the results of several experimental tests developed by Holcomb and Yu [12] and de Paula et al.[7]. It can be seen in this table that the efficiency of the connection increases when the connected length increases in longitudinal direction. These experimental results are represented together with the numerical results in the same Fig. 8(a), corroborating a similar tendency.

The effect of connected length in the transverse direction (L_t) on connection efficiency is also analyzed (see Fig. 7). Several numerical models utilizing cold-formed angle, with legs of 100 x 100 mm and thickness of 2.66 mm, bolted to the gusset plate with the same configuration of the Fig. 7 were developed. The L_t distance was increased between 30 and 60 mm and connection efficiency increased following a linear trend, as can be seen in Fig 8(b). A linear fit was developed, which has a coefficient R^2 of 0.976. The experimental results summarized in Table 3 and represented in the same Fig. 8(b) show similar behavior to numerical analyses.

5.2 Effect of eccentricity on connection efficiency

In this section, the effect of the eccentricities in $\bar{x}$ and $\bar{y}$ directions on connection efficiency is analyzed (see Fig. 7). The numerical models have virtual cold-formed angles with thickness legs of 2.66 mm and a bolt arrangement similar to the presented one in Fig. 7. The cold-formed angles dimensions (b_c and b_d) used in the numerical models are summarized in Table 4. The dimensions of these cold-formed angles are not commercial; they have been used in numerical models only with a purpose of the theoretical study.

As can be seen in Table 4, eccentricity $\bar{x}$ was increased from 7.4 to 43.7 mm, and a decrease in connection efficiency was observed. Fig. 9 (a) shows graphically the linear relationship between U_{FE} and $\bar{x}$, and as a verification way, a linear fit was developed, showing a coefficient R^2 of 0.994.

Table 4. Effect of eccentricity $\bar{x}$ on connection efficiency.

Source	Specimen	Number of bolt lines	Number of holes per bolt line	b_c - b_d (mm)	$\bar{x}$ (mm)	U_{FE}
FE analysis	11	2	2	150 – 50	7.4	0.514
	12			140 - 60	10.1	0.503
	13			130 – 70	13.4	0.497
	14			120 – 80	17.2	0.495
	15			110 - 90	21.5	0.476
	16			90 - 110	31.6	0.462
	17			80 - 120	37.4	0.440
	18			70 - 130	43.7	0.378

Note: The nominal bolt diameter and thickness legs for all models are 12.7 mm (1/2”) and 2.66 mm respectively.

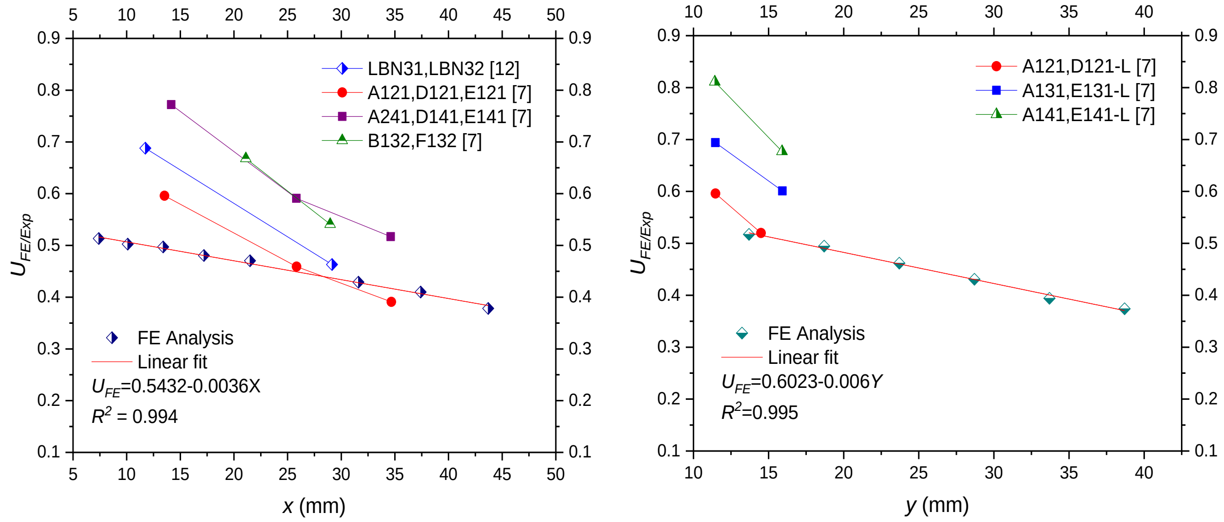

Fig. 9. Effect of eccentricity in: (a) The direction of $\bar{x}$ and (b) The direction of $\bar{y}$.

An analysis of experimental results to validate the previous numerical study was carried out, taken into account the real tests reported by Holcomb and Yu [12], and de Paula et al. [7]. Some of these results are summarized in Table 5, where an efficiency reduction is observed when the connection eccentricity in the $\bar{x}$ direction is increased. In the same Fig. 9 (a) the experimental results are presented together with the numerical results where a similar behavior between both is observed.

Table 5. Effect of eccentricity $\bar{x}$ and $\bar{y}$ in direction on connection efficiency.

Tested by	Specimen	Number of bolt lines	Number of holes per bolt line	b_c - b_d - t (mm)	$\bar{x}$ (mm)	$\bar{y}$ (mm)	$U_{exp}^{(1)}$
Holcomb and Yu [12]	LBN31	1	2	41.3 – 41.3 – 3.05	11.74	9.56	0.688 (*)
	LBN32			41.3 – 82.5 – 3.05	29.14	12.74	0.463(*)
de Paula et al. [7]	A121	1	2	50 – 50 – 2.23	13.53	11.47	0.596
	D121			50 – 80 – 2.41	25.84	13.90	0.459
	E121			50 – 100 – 2.49	34.67	15.00	0.391
	A241	1	4	50 – 50 – 3.57	14.15	10.85	0.772
	D141			50 – 80 – 2.36	25.82	13.93	0.591
	E141			50 – 100 – 2.38	34.61	15.08	0.517
	B132	2	3	80 – 80 – 2.43	21.11	18.89	0.668
	F132			80 – 100 – 2.48	28.97	20.84	0.541
de Paula et al. [7]	A121	1	2	50 – 50 – 2.23	13.53	11.47	0.596
	D121-L			80 – 50 – 2.29	10.61	14.50	0.520
	A131	1	3	50 – 50 – 2.26	13.54	11.46	0.694
	E131-L			100 – 50 – 2.25	9.29	15.92	0.601
	A141	1	4	50 – 50 – 2.34	13.58	11.42	0.811
	E141-L			100 – 50 – 2.29	9.31	15.90	0.677

Note: The nominal bolt diameter is 12.7 mm (1/2") for all specimens.
(*) Average in the series.

Effect of the eccentricity, in $\bar{y}$ direction, on connection efficiency is also analyzed numerically and experimentally in this section. Six numerical models utilizing cold-formed angles with legs of 100 x 100 mm and thickness of 2.66 mm were performed. The arrangement of the bolts in the connection is represented in Fig. 7. The distance between sequential bolts is 38.1 mm. The eccentricity $\bar{y}$ was increased from 13.7 to 38.7 mm. The connection efficiency vs. eccentricity $\bar{y}$ is graphically represented in Fig. 9 (b), where an efficiency reduction is observed when the eccentricity $\bar{y}$ is increased. It is also noted that the functional relationship between the connection efficiency and eccentricity $\bar{y}$ is linear (see Fig. 9(b)). Table 5 summarizes experimental results where a reduction of connection efficiency is observed when the eccentricity $\bar{y}$ increases. These results are represented in Fig. 9 (b) corroborating the linear trend of the numerical results.

6. New equation for the efficiency prediction of the net section area

In this section, a new equation for the efficiency prediction of the net section area is presented. The equation is developed using regression analysis and is based on a large number of experimental results reported in the literature by several authors [7,9,12,13] where all specimens showed net section failure. Table 6 summarizes the principal parameters of the experimental tests utilized for the analyses performed in this study. At the same time 160 numerical models were developed evidencing a net section failure in all cases. Table 7 shows the data and results of the numerical models.

In the previous section, it has been numerically verified that there is a linear relationship between the efficiency of the net section (U_{FE}) and each one of the variables studied individually (L, L_t, $\bar{x}$, and $\bar{y}$). In this section, Figs. 10 and 11 show the dispersion diagrams between the coefficient (U_{FE}) and the ratios: $\bar{x}/L$, $\bar{x}/L_t$, $\bar{y}/L$, and $\bar{y}/L_t$. In all cases, it has been observed that there is a quasi-linear relationship where U_{FE} decreases when $\bar{x}/L$, $\bar{x}/L_t$, $\bar{y}/L$, and $\bar{y}/L_t$ increase. Therefore, this fact corroborates the linear relationship between U_e and $\bar{x}/L$ proposed in the expression of Laboube and Yu [5] (see Fig. 10 (a)) and the possibility of arriving at a new prediction equation with a functional relationship similar to that of Laboube and Yu [5] that includes the new factors ($\bar{x}/L_t$, $\bar{y}/L$, and $\bar{y}/L_t$).

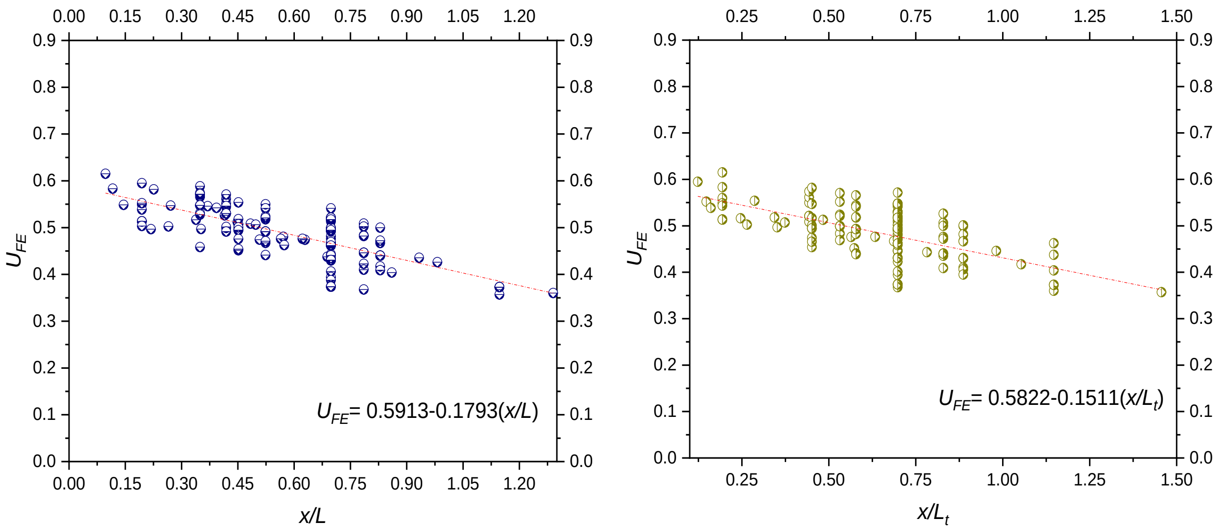

Fig. 10. Relationship dispersion diagrams: (a) U_{FE} vs. $\bar{x}/L$, and (b) U_{FE} vs. $\bar{x}/L_t$.

For the efficiency prediction of the net section area on bolted connections in cold-formed steel angles, Eq. (6) proposes the coefficient U_e. Such coefficient was obtained from a regression analysis using the SPSS software [20]. In this analysis, the R^2 coefficients for one bolt line and two bolt lines were 0.805 and 0.847 respectively.

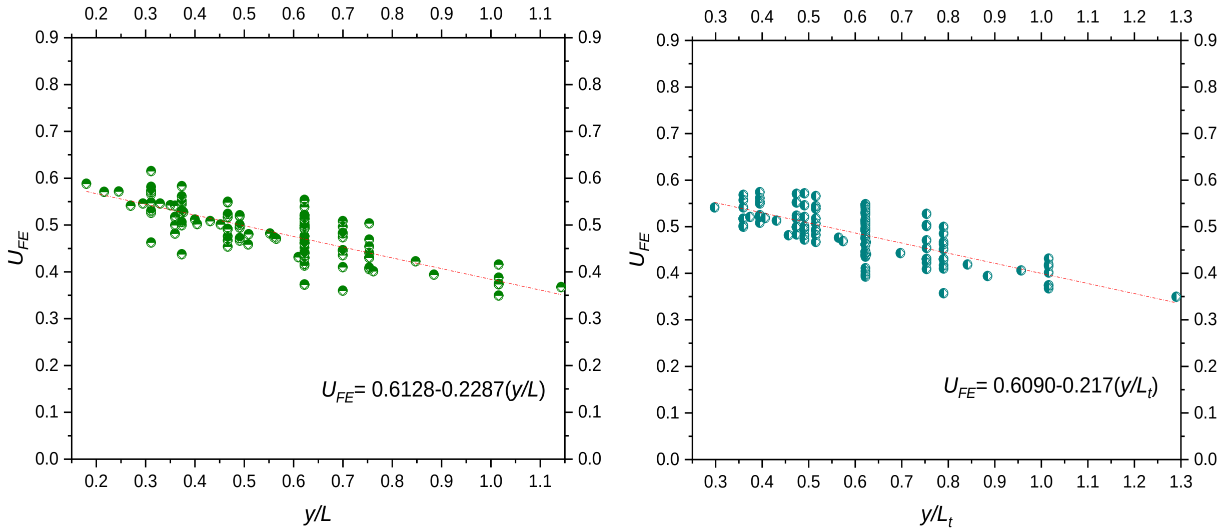

Fig. 11. Relationship dispersion diagrams: (a) U_{FE} vs. $\bar{y}/L$ and (b) U_{FE} vs. $\bar{y}/L_t$.

$$U_e = k_0 - k_1\frac{\bar{x}}{L} - k_2\frac{\bar{x}}{L_t} - k_3\frac{\bar{y}}{L} - k_4\frac{\bar{y}}{L_t} \tag{6}$$

where, the coefficients k_0, k_1, k_2, k_3, and k_4 are respectively 0.9, 0.2, 0.1, 0.26, and 0.05 for one bolt line and 0.9, 0.025, 0.2, 0.3, and 0.15 for two bolt lines. The distance L_t is taken as the nominal bolt diameter when one bolt line is used.

Therefore, in this study, the nominal resistance of the net section is determined by Eq. (7):

$$T_n = U_e \cdot A_n \cdot F_u \tag{7}$$

Eq. (6) is easy to apply and has a functional relationship similar to the equation proposed by Laboube and Yu [5]. Additionally, it should be noted that in the tests developed by Teh and Gilbert [9] and also utilized in this research to find the Eq. (6), G450 steel sheet was used, which exhibits less ductility than the material used by other authors, such as de Paula et al. [7]. An important feature in Eq. (6) is that it is not a unique general equation for U_e, like the ones proposed by [2–4,7,10]. Due to the variety of connections and variables, a unique general equation may be more feasible to errors. Instead, Eq.(6) can be changed (changing k_0, k_1, k_2, k_3, and k_4) according to the connection types and bolt distributions.

Table 6. Experimental tests utilized for regression analysis.

Tested by	Specimen	Number of bolt lines	Number of holes per bolt line	b_c - b_d (mm)	t (mm)	d (mm)	$\bar{x}$ (mm)	$\bar{y}$ (mm)	L (mm)	L_t (mm)
Holcomb and Yu [12]	LBN11, LCN11, LBN12, LCN12, LBN13, LCN13, LBN31, LCN31, LBN32, LCN32, LBN33, LCN33	1	2, 3	41.3–41.3 82.5-41.3 41.3–82.5	1.07 3.05	12.7	7.34, 8.2, 10.81, 11.74 29.14	9.56 13.58	38.1 76.2	-
Yip and Cheng [13]	l2.2, l2.3, l2.4, l4.2, l4.3, l6.2, l6.3, A2-2, A2-2N, A2-3, A3-2, A3-3, A4-2, A4-3, A4-4	1	2, 3, 4	38.1-38.1 50.8-50.8 51-51 76-76 102-102	1.21 1.52 1.90 2.66	12.7 15.9 19.1	10.22, 13.31 13.57, 19.55 26.05, 26.72	9.15 25.19	38.1 63.3 76.2 95.5 126.6 190.5 191	-
de Paula et al. [7]	A121, A131, A141, A221, A231, A241, A321, A331, A341, B131, B141, B221, B231, B241, B321, B331, B341, B122, B132, B142, B212, B222, B232, B242, C131, C141, C221, C231, C241, C331, C341, C122, C132, C142, C212, C222, C232, C242, C312, C322, C332, C342, D121, D131, D141, E121, E131, E141, F121, F131, F141, F122, F132, F142, D121-L, D131-L, D141-L, D112-L D122-L, D132-L, D142-L, E131-L, E141-L, E122-L, E132-L, E142-L	1 2	1, 2, 3, 4	50–50 50–80 50–100 80-50 80–80 80–100 100-50 100-100	2.21 2.23 2.25 2.26 2.27 2.29 2.34 2.36 2.38 2.41 2.43 2.48 2.49 2.66 3.49 3.35 3.51 3.58 3.57 3.70 3.75 3.84 3.85 3.86	12.7	9.30, 9.31, 34.72,10.57, 10.58,10.59, 10.61,13.53, 13.54,13.58, 14.12,14.13, 14.15,14.2, 14.22,14.23, 21.04, 21.1, 21.11,21.61, 21.62,21.63, 21.69,21.73, 21.76,21.78, 25.82,25.84, 25.85,26.03, 26.11,26.12, 26.17,26.22, 26.60,26.61, 26.64,26.65, 26.70,26.76, 26.77,26.78, 26.80,28.88, 28.9,28.92, 28.97,34.61, 34.67,34.72	10.77,10.78, 10.8,10.85, 10.87,10.88, 11.42,11.46, 13.9,13.93, 14.50,14.52, 14.53,14.95, 15.01,15.08, 15.9,15.91, 15.92,18.24, 18.21,18.27, 18.31,18.37, 18.38,18.39, 18.89,18.9, 18.96,20.84, 20.86,20.90, 20.92,20.94, 23.20,23.23, 23.3,23.35, 23.36,23.39, 23.78,23.83, 23.88,23.97, 37.34,47.32, 47.33	- 38.1 76.2 114.3	- 38.1
Teh and Gilbert [9]	EA1 to EA24 DEA1 to DEA9 AEA1 to AEA5 UAW1 to UAW11 UAW13,16,17,19 UAN1 to UAN12	1	2	40-40 40-60 40-80 50-50 50-75 50-100 60-60 60-40 75-75 75-50 80-40 100-50	1.5 3.0	12 16	6.45, 6.57, 7.8, 7.92, 8.11, 9.8, 9.92, 10.6, 10.7, 13.1, 13.2, 15.6, 15.7, 19.3, 19.5, 24, 28.3, 34.9	9.3, 9.4, 10.38, 10.5, 11.58, 11.7, 11.8, 11.9, 12.2, 13.38, 13.5, 14.3, 14.4, 15.1, 15.2, 16.89, 18.2,	40 50 60 75 80 100	-

Table 7. Numerical simulation results utilized for regression analysis.

No.	b_c (mm)	b_d (mm)	$\bar{x}$ (mm)	$\bar{y}$ (mm)	L (mm)	L_t (mm)	T_{FE} (kN)	U_{FE}	No.	b_c (mm)	b_d (mm)	$\bar{x}$ (mm)	$\bar{y}$ (mm)	L (mm)	L_t (mm)	T_{FE} (kN)	U_{FE}
1	100	100	26.6	23.7	33.87	38.1	99.52	0.446	26	100	100	26.6	23.7	38.1	38.1	103.02	0.462
2	100	100	26.6	23.7	42.29	38.1	105.75	0.474	27	120	80	17.2	23.7	38.1	38.1	110.36	0.495
3	100	100	26.6	23.7	46.57	38.1	107.17	0.480	28	150	50	7.4	23.7	38.1	38.1	114.53	0.513
4	100	100	26.6	23.7	50.8	38.1	109.64	0.491	29	70	130	43.7	23.7	50.8	38.1	90.13	0.404
5	100	100	26.6	23.7	54.99	38.1	113.43	0.508	30	90	110	31.6	23.7	50.8	38.1	106.21	0.476
6	100	100	26.6	23.7	59.27	38.1	114.16	0.512	31	100	100	26.6	23.7	50.8	38.1	109.64	0.491
7	100	100	26.6	23.7	63.5	38.1	118.28	0.530	32	120	80	17.2	23.7	50.8	38.1	115.29	0.517
8	100	100	26.6	23.7	67.69	38.1	120.99	0.542	33	150	50	7.4	23.7	50.8	38.1	122.38	0.548
9	100	100	26.6	23.7	71.97	38.1	121.79	0.546	34	70	130	43.7	23.7	63.5	38.1	97.64	0.438
10	100	100	26.6	23.7	76.2	38.1	122.17	0.548	35	90	110	31.6	23.7	63.5	38.1	112.98	0.506
11	150	50	7.4	23.7	38.1	38.1	114.53	0.514	36	100	100	26.6	23.7	63.5	38.1	118.28	0.530
12	140	60	10.1	23.7	38.1	38.1	112.12	0.503	37	120	80	17.2	23.7	63.5	38.1	122.04	0.547
13	130	70	13.4	23.7	38.1	38.1	110.88	0.497	38	150	50	7.4	23.7	63.5	38.1	130.10	0.583
14	120	80	17.2	23.7	38.1	38.1	110.36	0.481	39	70	130	43.7	23.7	76.2	38.1	103.20	0.463
15	110	90	21.5	23.7	38.1	38.1	106.21	0.470	40	90	110	31.6	23.7	76.2	38.1	117.38	0.526
16	90	110	31.6	23.7	38.1	38.1	98.16	0.429	41	100	100	26.6	23.7	76.2	38.1	122.17	0.548
17	80	120	37.4	23.7	38.1	38.1	106.21	0.410	42	120	80	17.2	23.7	76.2	38.1	129.78	0.582
18	70	130	43.7	23.7	38.1	38.1	83.18	0.378	43	150	50	7.4	23.7	76.2	38.1	137.25	0.615
19	70	130	43.7	23.7	33.87	38.1	80.32	0.360	44	100	100	26.6	23.7	38.1	30	95.97	0.430
20	90	110	31.6	23.7	33.87	38.1	97.17	0.436	45	100	100	26.6	23.7	38.1	34	98.88	0.443
21	100	100	26.6	23.7	33.87	38.1	99.52	0.446	46	100	100	26.6	23.7	38.1	42	106.27	0.476
22	120	80	17.2	23.7	33.87	38.1	105.78	0.474	47	100	100	26.6	23.7	38.1	46	109.93	0.493
23	150	50	7.4	23.7	33.87	38.1	110.77	0.496	48	100	100	26.6	23.7	38.1	50	111.38	0.499
24	70	130	43.7	23.7	38.1	38.1	83.18	0.373	49	100	100	26.6	23.7	38.1	55	114.45	0.513
25	90	110	31.6	23.7	38.1	38.1	98.16	0.440	50	100	100	26.6	23.7	38.1	60	116.26	0.521

Table 7 (continued)

No.	b_c (mm)	b_d (mm)	$\bar{x}$ (mm)	$\bar{y}$ (mm)	L (mm)	L_t (mm)	T_{FE} (kN)	U_{FE}	No.	b_c (mm)	b_d (mm)	$\bar{x}$ (mm)	$\bar{y}$ (mm)	L (mm)	L_t (mm)	T_{FE} (kN)	U_{FE}
51	100	100	26.6	13.7	38.1	38.1	115.38	0.517	76	100	100	26.6	23.7	76.2	30	118.47	0.531
52	100	100	26.6	18.7	38.1	38.1	110.36	0.495	77	100	100	26.6	23.7	76.2	38.1	122.17	0.548
53	100	100	26.6	28.7	38.1	38.1	96.08	0.431	78	100	100	26.6	23.7	76.2	46	126.22	0.566
54	100	100	26.6	33.7	38.1	38.1	87.93	0.394	79	100	100	26.6	23.7	76.2	50	127.29	0.571
55	100	100	26.6	38.7	38.1	38.1	83.44	0.374	80	100	100	26.6	23.7	76.2	60	128.09	0.574
56	100	100	26.6	23.7	33.87	30	91.48	0.410	81	70	130	43.7	23.7	38.1	30	79.68	0.357
57	100	100	26.6	23.7	33.87	38.1	99.52	0.446	82	70	130	43.7	23.7	38.1	38.1	83.18	0.373
58	100	100	26.6	23.7	33.87	46	107.61	0.482	83	90	110	31.6	23.7	38.1	30	93.05	0.417
59	100	100	26.6	23.7	33.87	50	107.82	0.483	84	90	110	31.6	23.7	38.1	38.1	98.16	0.440
60	100	100	26.6	23.7	33.87	60	113.46	0.509	85	90	110	31.6	23.7	38.1	46	104.22	0.467
61	100	100	26.6	23.7	38.1	30	95.97	0.430	86	100	100	26.6	23.7	38.1	30	95.97	0.430
62	100	100	26.6	23.7	38.1	38.1	103.02	0.462	87	100	100	26.6	23.7	38.1	38.1	103.02	0.462
63	100	100	26.6	23.7	38.1	46	109.93	0.493	88	100	100	26.6	23.7	38.1	46	109.93	0.493
64	100	100	26.6	23.7	38.1	50	111.38	0.499	89	100	100	26.6	23.7	38.1	50	111.38	0.499
65	100	100	26.6	23.7	38.1	60	116.26	0.521	90	100	100	26.6	23.7	38.1	60	116.26	0.521
66	100	100	26.6	23.7	50.8	30	104.25	0.467	91	120	80	17.2	23.7	38.1	30	100.75	0.452
67	100	100	26.6	23.7	50.8	38.1	109.64	0.491	92	120	80	17.2	23.7	38.1	38.1	110.36	0.495
68	100	100	26.6	23.7	50.8	46	115.51	0.518	93	120	80	17.2	23.7	38.1	46	113.11	0.507
69	100	100	26.6	23.7	50.8	50	116.87	0.524	94	120	80	17.2	23.7	38.1	50	115.56	0.518
70	100	100	26.6	23.7	50.8	60	122.66	0.550	95	120	80	17.2	23.7	38.1	60	123.58	0.554
71	100	100	26.6	23.7	63.5	30	111.44	0.499	96	150	50	7.4	23.7	38.1	30	103.15	0.462
72	100	100	26.6	23.7	63.5	38.1	118.28	0.530	97	150	50	7.4	23.7	38.1	38.1	114.53	0.513
73	100	100	26.6	23.7	63.5	46	121.39	0.544	98	150	50	7.4	23.7	38.1	46	120.17	0.539
74	100	100	26.6	23.7	63.5	50	123.12	0.552	99	150	50	7.4	23.7	38.1	50	123.21	0.552
75	100	100	26.6	23.7	63.5	60	125.28	0.561	100	150	50	7.4	23.7	38.1	60	132.71	0.595

Table 7 (continued)

No.	b_c (mm)	b_d (mm)	$\bar{x}$ (mm)	$\bar{y}$ (mm)	L (mm)	L_t (mm)	T_{FE} (kN)	U_{FE}	No.	b_c (mm)	b_d (mm)	$\bar{x}$ (mm)	$\bar{y}$ (mm)	L (mm)	L_t (mm)	T_{FE} (kN)	U_{FE}
101	100	100	26.6	13.7	33.87	38.1	112.04	0.502	126	100	100	26.6	13.7	38.1	30	107.50	0.482
102	100	100	26.6	18.7	33.87	38.1	107.56	0.482	127	100	100	26.6	18.7	38.1	30	104.10	0.467
103	100	100	26.6	23.7	33.87	38.1	99.52	0.446	128	100	100	26.6	23.7	38.1	30	95.97	0.430
104	100	100	26.6	28.7	33.87	38.1	94.29	0.423	129	100	100	26.6	28.7	38.1	30	90.61	0.406
105	100	100	26.6	38.7	33.87	38.1	82.04	0.368	130	100	100	26.6	38.7	38.1	30	77.96	0.349
106	100	100	26.6	13.7	38.1	38.1	115.38	0.517	131	100	100	26.6	13.7	38.1	38.1	115.38	0.517
107	100	100	26.6	18.7	38.1	38.1	110.36	0.495	132	100	100	26.6	18.7	38.1	38.1	110.36	0.495
108	100	100	26.6	23.7	38.1	38.1	103.02	0.462	133	100	100	26.6	23.7	38.1	38.1	103.02	0.462
109	100	100	26.6	28.7	38.1	38.1	96.08	0.431	134	100	100	26.6	28.7	38.1	38.1	96.08	0.431
110	100	100	26.6	38.7	38.1	38.1	83.44	0.374	135	100	100	26.6	38.7	38.1	38.1	83.44	0.374
111	100	100	26.6	13.7	50.8	38.1	120.75	0.541	136	100	100	26.6	13.7	38.1	46	120.76	0.541
112	100	100	26.6	18.7	50.8	38.1	116.22	0.521	137	100	100	26.6	18.7	38.1	46	115.72	0.519
113	100	100	26.6	23.7	50.8	38.1	109.64	0.491	138	100	100	26.6	23.7	38.1	46	109.93	0.493
114	100	100	26.6	28.7	50.8	38.1	105.06	0.471	139	100	100	26.6	28.7	38.1	46	98.31	0.441
115	100	100	26.6	38.7	50.8	38.1	89.57	0.401	140	100	100	26.6	38.7	38.1	46	86.49	0.388
116	100	100	26.6	13.7	63.5	38.1	127.35	0.571	141	100	100	26.6	18.7	38.1	50	116.25	0.521
117	100	100	26.6	18.7	63.5	38.1	121.82	0.546	142	100	100	26.6	23.7	38.1	50	111.38	0.499
118	100	100	26.6	23.7	63.5	38.1	118.28	0.530	143	100	100	26.6	28.7	38.1	50	104.66	0.469
119	100	100	26.6	28.7	63.5	38.1	111.88	0.501	144	100	100	26.6	23.7	38.1	60	116.26	0.521
120	100	100	26.6	38.7	63.5	38.1	96.26	0.431	145	90	110	31.6	13.7	38.1	38.1	111.53	0.500
121	100	100	26.6	13.7	76.2	38.1	131.25	0.588	146	100	100	26.6	13.7	38.1	38.1	115.38	0.517
122	100	100	26.6	18.7	76.2	38.1	127.53	0.572	147	90	110	31.6	18.7	38.1	38.1	105.37	0.472
123	100	100	26.6	23.7	76.2	38.1	122.17	0.548	148	100	100	26.6	18.7	38.1	38.1	110.36	0.495
124	100	100	26.6	28.7	76.2	38.1	117.72	0.528	149	120	80	17.2	18.7	38.1	38.1	111.73	0.501
125	100	100	26.6	38.7	76.2	38.1	102.29	0.458	150	70	130	43.7	23.7	38.1	38.1	83.18	0.373

Table 7 (continued)

No.	b_c (mm)	b_d (mm)	$\bar{x}$ (mm)	$\bar{y}$ (mm)	L (mm)	L_t (mm)	T_{FE} (kN)	U_{FE}
151	90	110	31.6	23.7	38.1	38.1	98.16	0.440
152	100	100	26.6	23.7	38.1	38.1	103.02	0.462
153	120	80	17.2	23.7	38.1	38.1	110.36	0.495
154	150	50	7.4	23.7	38.1	38.1	114.53	0.513
155	90	110	31.6	28.7	38.1	38.1	91.25	0.409
156	100	100	26.6	28.7	38.1	38.1	96.08	0.431
157	120	80	17.2	28.7	38.1	38.1	101.32	0.454
158	150	50	7.4	28.7	38.1	38.1	112.36	0.504
159	100	100	26.6	38.7	38.1	38.1	83.44	0.374
160	120	80	17.2	38.7	38.1	38.1	92.74	0.416

Note: In all numerical models, the bolt diameter, thickness of cold-formed angle, number of bolt lines and number of holes per bolt line are equal to 12.7 mm, 2.66 mm, 2 and 2 respectively.

7. Verification of the accuracy in the prediction of the nominal resistance of the net section

Previously, a new equation, Eq. (6), for the efficiency prediction of the net section area was presented. In this section, the prediction results of the nominal resistance (same approach done in [7,15,21,22]) of the net section given by the codes AISI [10], Eurocode-3 [11] and using Eq. (7) are compared with experimental results reported in the literature by [7,9,12,13]. Some test parameters from these experimental studies are shown in Table 6.

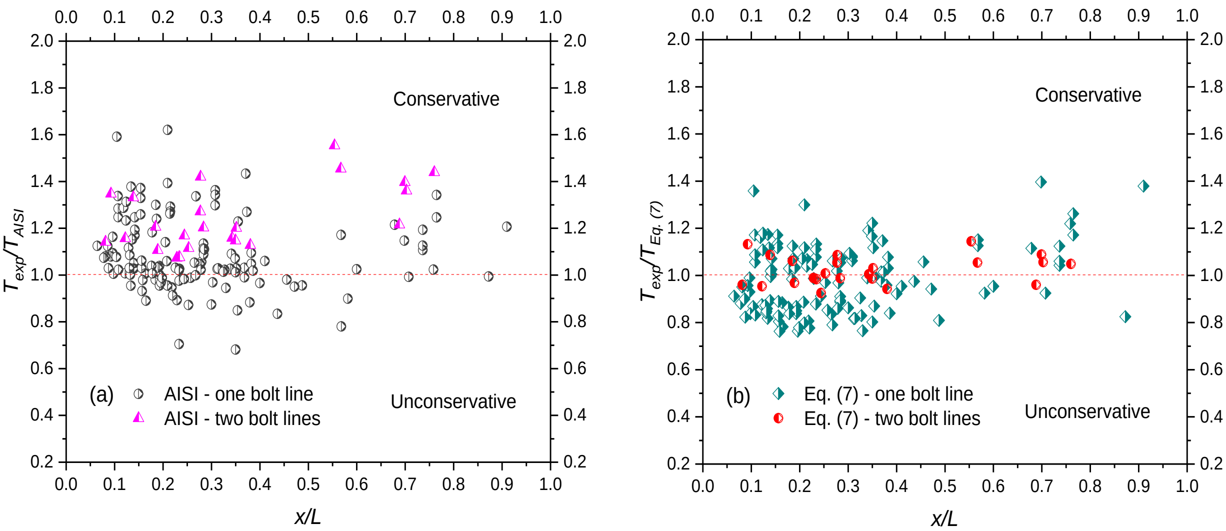

(a) T_{exp}/T_{AISI} vs. $\bar{x}/L$ ratio (b) $T_{exp}/T_{Eq.\ (7)}$ vs. $\bar{x}/L$ ratio

Fig. 12. Prediction of the nominal resistance of the net section according to AISI [10] and using Eq. (7), considering the relationships T_{exp}/T_{AISI} vs. $\bar{x}/L$ and $T_{exp}/T_{Eq.\ (7)}$ vs. $\bar{x}/L$.

The ratios T_{exp}/T_{AISI} and $T_{exp}/T_{Eq.\ (7)}$ obtained utilizing the AISI [10] code and using Eq. (7) are graphically shown in Figs 12 and 13. In Fig. 12, the relationships T_{exp}/T_{AISI} vs. $\bar{x}/L$ and $T_{exp}/T_{Eq.\ (7)}$ vs. $\bar{x}/L$ are presented. It is observed that the prediction according to AISI [10] code tends to give excessively conservative values of the nominal resistance of the net section in some cases - mainly when two bolt lines are used. Fig. 13 shows the relationships T_{exp}/T_{AISI} vs. $\bar{y}/L$ and $T_{exp}/T_{Eq.\ (7)}$ vs. $\bar{y}/L$ where the same trend can also be observed.

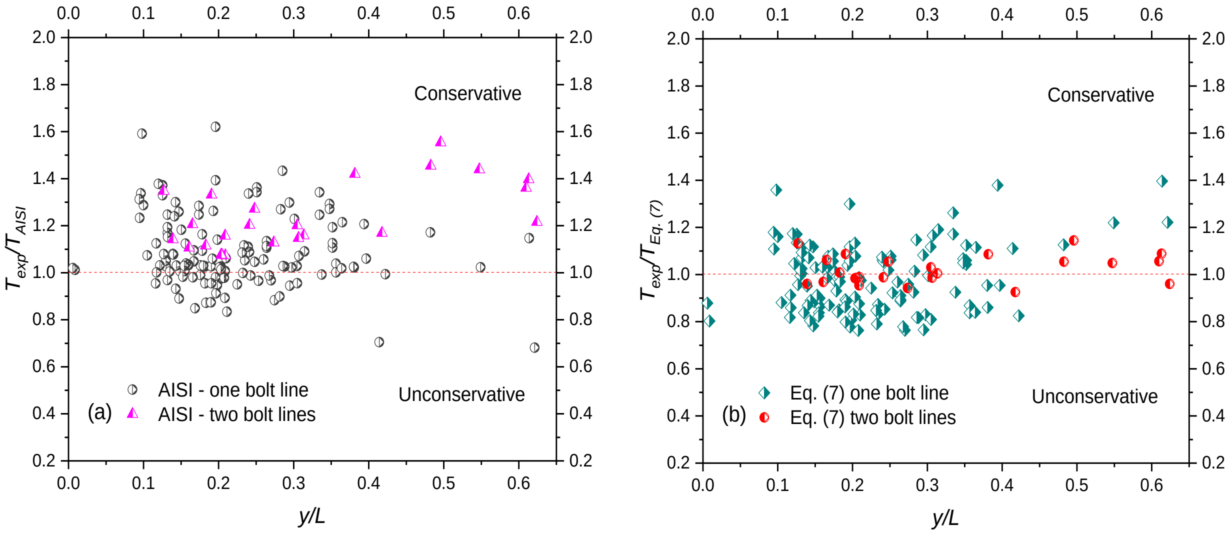

(a) T_{exp}/T_{AISI} vs. $\bar{y}/L$ ratio (b) $T_{exp}/T_{Eq.\ (7)}$ vs. $\bar{y}/L$ ratio

Fig. 13 Prediction of the nominal resistance of the net section according to AISI [10] and using Eq. (7), considering the relationships T_{exp}/T_{AISI} vs. $\bar{y}/L$ and $T_{exp}/T_{Eq.\ (7)}$ vs. $\bar{y}/L$.

In Figs. 14 and 15 the ratios $T_{exp}/T_{EC\text{-}3}$ and $T_{exp}/T_{Eq.\ (7)}$ are presented graphically. The relationships $T_{exp}/T_{EC\text{-}3}$ vs. $\bar{x}/L$ and $T_{exp}/T_{Eq.\ (7)}$ vs. $\bar{x}/L$ are shown in Fig. 14. It should be noted that Eurocode-3 [11] code tends to underestimate and overestimate the nominal resistance of the net section in several cases when one bolt line is used.

The relationships $T_{exp}/T_{EC\text{-}3}$ vs. $\bar{y}/L$ and $T_{exp}/T_{Eq.\ (7)}$ vs. $\bar{y}/L$, are presented in Fig. 15, exhibiting the same trend as illustrated in Fig. 14. Figs. 12, 13, 14 y 15 also show that AISI [10] and Eurocode-3 [11] specifications offer more scattered results than those obtained with the application of Eq. (7), with U_e obtained from Eq. (6).

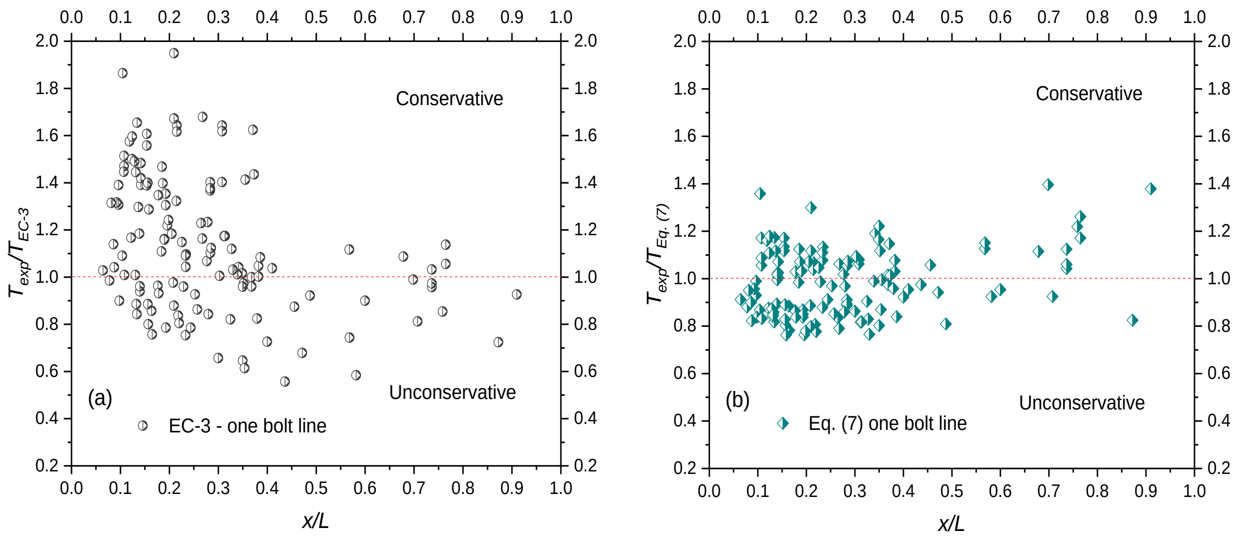

(a) $T_{exp}/T_{EC\text{-}3}$ vs. $\bar{x}/L$ ratio (b) $T_{exp}/T_{Eq.\ (7)}$ vs. $\bar{x}/L$ ratio

Fig. 14 Prediction of the nominal resistance of the net section according to EC-3 [11] and using Eq. (7), considering the relationships $T_{exp}/T_{EC\text{-}3}$ vs. $\bar{x}/L$ and $T_{exp}/T_{Eq.\ (7)}$ vs. $\bar{x}/L$.

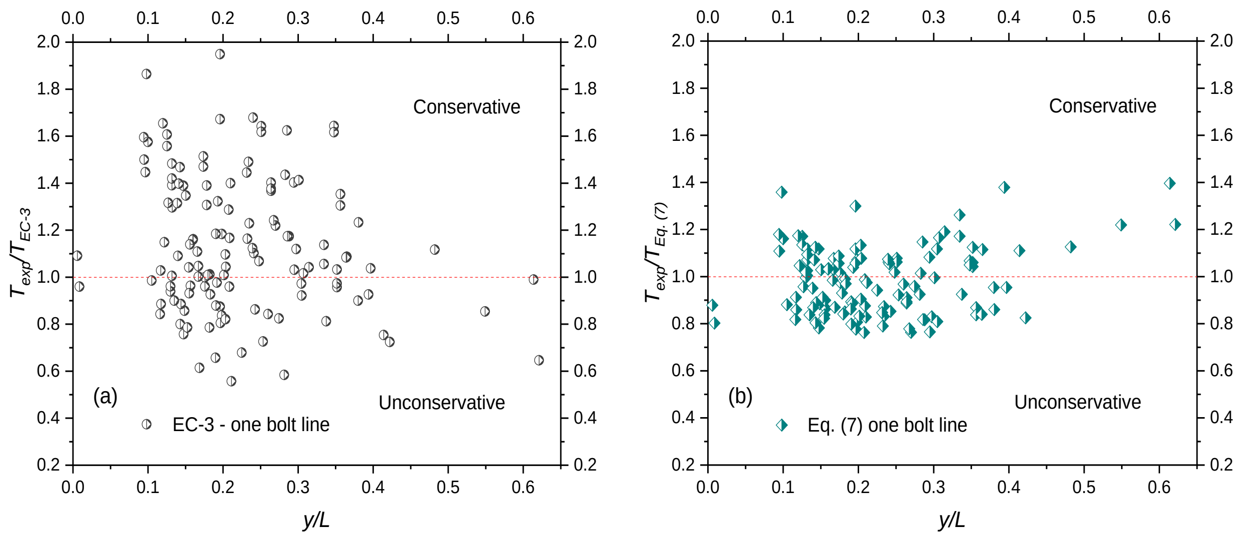

(a) $T_{exp}/T_{EC\text{-}3}$ vs. $\bar{y}/L$ ratio (b) $T_{exp}/T_{Eq.\ (7)}$ vs. $\bar{y}/L$ ratio

Fig. 15 Prediction of the nominal resistance of the net section according to EC-3 [11] and using Eq. (7), considering the relationships $T_{exp}/T_{EC\text{-}3}$ vs. $\bar{y}/L$ and $T_{exp}/T_{Eq.\ (7)}$ vs. $\bar{y}/L$.

Table 8 summarizes statistical data with the results of the comparison between the nominal resistance of the net section (T_{AISI}, $T_{EC\text{-}3}$, and $T_{Eq.\ (7)}$) and experimental tests [7,9,12,13]. It should be highlighted that the above mentioned comparison is made using only experimental results reported in the literature (see Table 6). For connection with one bolt line, the mean values ratios of T_{exp}/T_{AISI}, $T_{exp}/T_{EC\text{-}3}$, and $T_{exp}/ T_{Eq.\ (7)}$ are, respectively, 1.088, 1.234, and 0.986 with their corresponding COV (coefficient of variation) of 0.144, 0.225, and 0.138, respectively. It should be pointed out that using Eq. (7) leads to the value of the ratio $T_{exp}/ T_{Eq.}$

$_{(7)}$ equal to 0.986, very close to 1.0, and to the lowest COV value equal to 0.138. The ratios of T_{exp} / $T_{AISI\ /\ EC\text{-}3\ /\ Eq.\ (7)}$ > 1.2 indicate that AISI [10] and Eurocode-3 [11] are conservative in several cases: 22.4% for T_{exp}/T_{AISI} and 47.6% for $T_{exp}/T_{EC\text{-}3}$ showing that T_{AISI} and $T_{EC\text{-}3}$ are much less than the expected T_{exp} values.

Table 8. Statistical data from results generated using different procedures.

	One bolt line			Two bolt lines	
Statistical parameters	T_{exp} / T_{AISI}	T_{exp} / $T_{EC\text{-}3}$	T_{exp} / $T_{Eq.(7)}$	T_{exp} / T_{AISI}	T_{exp} / $T_{Eq.(7)}$
Mean	1.088	1.234	0.986	1.240	1.021
Maximum Value	1.620	1.949	1.396	1.554	1.145
Minimum Value	0.682	0.646	0.763	1.073	0.925
Coefficient of Variation	0.144	0.225	0.138	0.112	0.059
T_{exp} / $T_{AISI\ /\ EC\text{-}3\ /\ Eq.\ (7)}$ < 0.8 (%)	3.0	3.6	6.1	0.0	0.0
0.8 < T_{exp} / $T_{AISI\ /\ EC\text{-}3\ /\ Eq.\ (7)}$ < 1 (%)	23.1	17.9	48.1	0.0	45.8
1 < T_{exp} / $T_{AISI\ /\ EC\text{-}3\ /\ Eq.\ (7)}$ < 1.2 (%)	51.5	30.9	40.5	44.7	54.2
T_{exp} / $T_{AISI\ /\ EC\text{-}3\ /\ Eq.\ (7)}$ > 1.2 (%)	22.4	47.6	5.3	55.3	0.0

Note: The verification of the codes AISI [10] and EC-3 [11], as well as using Eq. (7) is made utilizing only the experimental results [7,9,12,13].

For connection with two bolt lines the mean values of T_{exp}/T_{AISI} and $T_{exp}/\ T_{Eq.\ (7)}$ ratios are 1.24 and 1.021, respectively. The COVs for T_{exp}/T_{AISI} and $T_{exp}/\ T_{Eq.\ (7)}$ ratios are, respectively, 0.112 and 0.059. It is observed a very low COV value for the ratio $T_{exp}/\ T_{Eq.\ (7)}$. Consequently, the ratios T_{exp} / $T_{AISI\ /\ EC\text{-}3\ /\ Eq.\ (7)}$ < 0.8 and T_{exp} / $T_{AISI\ /\ EC\text{-}3\ /\ Eq.\ (7)}$ > 1.2 are equal to zero for the prediction using Eq. (7). However, for the prediction using AISI [10], the ratio T_{exp} / $T_{AISI\ /\ EC\text{-}3\ /\ Eq.\ (7)}$ > 1.2 is 55.3%, showing that T_{AISI} is much less than the expected T_{exp} values. It is appreciated that the trend of AISI [10] is to underestimate the nominal resistance of the net section for connection with two bolt lines.

Taking into consideration the results of the verification of the methods analyzed [10,11] and using Eq. (7), it can be concluded that U_e value obtained from Eq. (6), proposed in this research, improves the prediction of the nominal resistance of the net section of bolted connections in cold-formed angles. The proposed equation for the prediction of the net section resistance (nominal value), compared to experimental data (according to Table 8) resulted in a coefficient of variation COV = 0.138 (for one bolted line) and COV = 0.059 (for two bolted lines). However, for AISI, COV = 0.144 (for one bolted line) and 0.112 (for two bolted lines); and for Eurocode-3, COV = 0.225 (for one bolted line). For the AISI, the ratio between experimental (T_{exp}) and predicted net section resistance (T_{AISI}), respectively, for maximum and minimum values are: T_{exp} /T_{AISI} = 1.620 and T_{exp} /T_{AISI} = 0.682 (for one bolted line), and, T_{exp} /T_{AISI} = 1.554 and T_{exp} /T_{AISI} = 1.073 (for two bolted line). For Eurocode, maximum and minimum values are, respectively, T_{exp} /$T_{EC\text{-}3}$ = 1.940 and T_{exp} /$T_{EC\text{-}3}$ = 0.646. Also, examining Figures 12 to 15, it is also observed that the proposed equation, Eq. (6) (used in Eq.7), in this paper, shows less scattering than AISI [10] and Eurocode-3 [11].

It is important to notice that Eq. (6) predicts the efficiency factor "U_e" for the net section resistance. Eq.(6) was used in Eq.(7) without any safety factor for design, as it compares nominal values: predicted vs. experimental. The goal of this article is not to replace AISI [10] nor Eurocode-3 [11] design equations, but to suggest a different approach for "U" used to calculate the nominal resistance. Notice that the proposed equation is much easier to be updated according to the increase of data base (numerical or experimental) or according to the type of connection of cold-formed angle section under tension. Eq. (6) also considers new factors ($\bar{x}/L_t$, $\bar{y}/L$, and $\bar{y}/L_t$) other than $\bar{x}/L$ suggested by Laboube and Yu [5], traditionally used.

8. Conclusions

Accurate nonlinear finite element models have been developed to investigate the efficiency variation due to shear lag in bolted connections of cold-formed angle section members under tension. The results obtained from FE analyses have been verified against experimental results and it has been demonstrated that the numerical models successfully predict the bolted connection resistance and the load-displacement behavior of the tests. Parametric studies have been conducted to investigate the effects on the efficiency coefficient of the connections by changing the distances L and L_t, being L the distance between adjacent bolts in the longitudinal direction (the same as that of the applied load) and L_t in the transverse direction. The nominal resistances of the net section of bolted connections calculated using AISI [10] and Eurocode-3 [11] have been verified against the test results carried out by various researchers. At least for the cases analyzed in this research, it can be concluded that: (a) the AISI [10] procedure has a trend to underestimate the nominal resistance of the net section mainly when two bolt lines are utilized; and (b) Eurocode-3 [11] offers very scattered results, with some of the nominal resistances of the net section underestimated or overestimated in several cases.

Therefore, a new equation, Eq. (6), is proposed to determine the efficiency reduction coefficient due to shear lag. With such equation, which is simple and easy to use, there is an improvement in the prediction of the nominal resistance of the net section $T_{Eq.(7)}$ compared to experimental results T_{exp}. For connection with one bolt line, the mean value and the coefficient of variation of the $T_{exp}/T_{Eq.(7)}$ ratio are 0.986 and 0.138, respectively. For connection with two bolt lines the mean value and the coefficient of variation of the $T_{exp}/T_{Eq.(7)}$ ratio are 1.021 and 0.059, respectively.

Acknowledgements

Authors are very thankful to CAPES (Brazilian Coordination for the Improvement of Higher Education Personnel) and CNPq (National Council for Scientific and Technological Development) for the financial support for this research.

9. References

[1] W.H. Munse, E.J. Chesson, Riveted and bolted joints: net section design, J. Struct. Div., ASCE. 89 (1963) 107–126.

[2] AISI(American Iron and Steel Institute), North American Specification for the Design

of Cold-Formed Steel Structural Members, (2001).

[3] AISI(American Iron and Steel Institute), North American Specification for the Design of Cold-Formed Steel Structural Members, (2010).

[4] AS/NZS-4600-2005, Cold-formed steel structures, (2005).

[5] R. Laboube, W.W. Yu, Tensile and bearing capacities of bolted connections. Final summary reports. Civil Egineering Study 95-6, University of Missouri - Rolla, 1995.

[6] G.L. Kulak, Y.E. Wu, Shear Lag in Bolted Angle Tension Members, Journal of Structural Engineering. 123 (1997) 1144–1152.

[7] V.F. de Paula, L.M. Bezerra, W.T. Matias, Efficiency reduction due to shear lag on bolted cold-formed steel angles, Journal of Constructional Steel Research. 64 (2008) 571–583.

[8] L.H. Teh, V. Yazici, Shear lag and eccentricity effects of bolted connections in cold-formed steel section, Engineering Structures. 52 (2013) 536–544.

[9] L.H. Teh, B.P. Gilbert, Net section tension capacity of cold-reduced sheet steel angle braces bolted at one leg, Journal of Structural Engineering. 139 (2013) 328–337.

[10] AISI (American Iron and Steel Institute), North American Specification for the Design of Cold-Formed Steel Structural Members, (2016).

[11] CEN (European Committee for Standardization), Design of steel structures – part 1-8: design of joints, Eurocode 3. (2005).

[12] B.D. Holcomb, W.W. Yu, Tensile and bearing capacities of bolted connections. Second summary report. Civil Engineering Study 95-1, University of Missouri-Rolla, 1995.

[13] A.S.M. Yip, J.J.R. Cheng, Shear lag in bolted cold-formed steel angles and channels in tension. Structural engineering report no. 233, Edmonton, Canada: University of Alberta, 2000.

[14] ABAQUS, User's Manual, Version 6.14-1, Dassault Systèmes Simulia Corp, Providence, RI, USA, 2014.

[15] L.H. Teh, B.P. Gilbert, Net Section Tension Capacity of Equal Angle Braces Bolted at Different Legs, Journal of Structural Engineering. 140 (2014) 6014002. doi:10.1061/(ASCE)ST.1943-541X.0000964.

[16] ABAQUS, Theory manual, Version 6.14-1, Dassault Systèmes Simulia Corp, Providence, RI, USA, 2014.

[17] V. de Paula, Análise experimental e numérica de cantoneiras de aço formadas a frio, sob tração e conectadas por parafusos, University of Brasilia, 2006.

[18] C. Fang, M.C.H. Yam, X. Zhou, Y. Zhang, Post-buckling resistance of gusset plate

connections: Behaviour, strength, and design considerations, Engineering Structures. 99 (2015) 9–27.

[19] E.L. Salih, L. Gardner, D.A. Nethercot, Numerical study of stainless steel gusset plate connections, Engineering Structures. 49 (2013) 448–464.

[20] SPSS-Inc, Guía breve de SPSS 15.0, SPSS Inc, Chicago, IL 60606-6412 EE.UU, 2006.

[21] J. Bonilla, L.M. Bezerra, E. Mirambell, B. Massicotte, Review of stud shear resistance prediction in steel-concrete composite beams, Steel and Composite Structures. 27 (2018) 355–370. doi:10.12989/scs.2018.27.3.355.

[22] J. Qureshi, D. Lam, J. Ye, The influence of profiled sheeting thickness and shear connector's position on strength and ductility of headed shear connector, Engineering Structures. 33 (2011) 1643–1656. doi:10.1016/j.engstruct.2011.01.035.